Uniaxial strain-modulated electronic structures of CdX (X = S, Se, Te) from first-principles calculations: A comparison between bulk and nanowires*

Linlin Xiang(相琳琳) and Shenyuan Yang(杨身园)†

State Key Laboratory of Superlattices and Microstructures, Institute of Semiconductors, Chinese Academy of Sciences, Beijing 100083, *China*

(Received 10 March 2017; revised manuscript received 4 May 2017; published online 20 June 2017)

Using first-principles calculations based on density functional theory, we systematically study the structural deformation and electronic properties of wurtzite CdX (X = S, Se, Te) bulk and nanowires (NWs) under uniaxial [0001] strain. Due to the intrinsic shrinking strain induced by surface contraction, large NWs with $\{10\bar{1}0\}$ facets have heavy hole (HH)-like valence band maximum (VBM) states, while NWs with $\{11\bar{2}0\}$ facets have crystal hole (CH)-like VBM states. The external uniaxial strain induces an HH–CH band crossing at a critical strain for both bulk and NWs, resulting in nonlinear variations in band gap and hole effective mass at VBM. Unlike the bulk phase, the critical strain of NWs highly depends on the character of the VBM state in the unstrained case, which is closely related to the size and facet of NWs. The critical strain of bulk is at compressive range, while the critical strain of NWs with HH-like and CH-like VBM appears at compressive and tensile strain, respectively. Due to the HH–CH band crossing, the charge distribution of the VBM state in NWs can also be tuned by the external uniaxial strain. Despite the complication of the VBM state, the electron effective mass at conduction band minimum (CBM) of NWs shows a linear relation with the CBM–HH energy difference, the same as the bulk material.

Keywords: first-principles calculations, electronic properties, semiconductor nanowires, uniaxial strain

PACS: 71.15.Mb, 73.22.–f, 73.61.Ga, 77.80.bn **DOI:** 10.1088/1674-1056/26/8/087103

1. Introduction

Nanoscale structures and heterostructures based on II–VI CdX (X = S, Se, Te) compounds have been widely studied in the past decades for their potential use in light-harvesting applications.[1–5] In the bulk phases, CdX compounds have direct band gaps well-matched to the solar spectrum[6] and exhibit good light absorption and emission.[1–5] According to their bulk band structures,[7,8] the CdSe/CdS interface is expected to exhibit type-I level alignment that could improve the photoluminescence quantum yield,[2] while the CdSe/CdTe and CdS/CdTe interfaces exhibit type-II level alignment that could facilitate charge separation, ideal for photovoltaic applications.[9,10] Due to the large lattice mismatch (e.g., 9.5% mismatch between CdS and CdTe), significant strain is expected to alter the band gap, band offsets, and other electronic properties of these heterostructures.

Strain engineering is an effective way to tune the structural, electronic, and optical properties of semiconductors and nanostructures.[11–15] It has been well known that strain can modulate the band gap, effective mass, and carrier mobility of bulk Si, Ge, and alloys, as an applicable method to improve the performance of Si/Ge-based electronic and optoelectronic devices.[11–13] At the nanoscale, heterostructures can potentially tolerate larger lattice-mismatch than the bulk heterojunctions.[16–18] Experimentally, high quality nanoscale heterostructures with lattice mismatch up to 19.8% have been successfully synthesized, and show strain-tunable level alignment and light emission with high quantum efficiency.[16] The resulting strain in the nanoscale heterostructures could be large and highly anisotropic. The interplay between strain and quantum confinement broadens the tunability on the properties of nanoscale materials.[16,19]

Although the strain-induced changes in the structural and electronic properties for bulk semiconductors have been widely studied, the strain effect on the nanostructures is still not well understood. The $\boldsymbol{k}\cdot\boldsymbol{p}$ effective mass model has been extensively used to explain the experimental measurements on quantum dots and nanoscale heterostructures,[2,20–22] but does not explicitly account for lattice strain. The continuum elastic model yields the structural deformation of nanoscale heterostructures using the bulk elastic parameters,[16,18] but cannot give atomic structure details and the detailed electronic structures. The tight-binding method can predict electronic structures,[23] but cannot perform structural relaxation. Moreover, all the above methods employ (unstrained) bulk parameters from experiments or first-principles calculations, since almost no parameter for nanostructures is available. It is questionable whether these bulk parameters are valid for the nanoscale lattice-mismatched heterostructures with small size

*Project supported by the National Natural Science Foundation of China (Grant Nos. 11204296 and 61427901) and the National Basic Research Program of China (Grant Nos. 2014CB643902 and 2013CB933304).

†Corresponding author. E-mail: syyang@semi.ac.cn

© 2017 Chinese Physical Society and IOP Publishing Ltd

and large strain. More accurate first-principles calculations can in principle predict both structural deformation and electronic properties of nanoscale materials.[19,24] However, previous studies have been focused on the strain-induced changes in band gap and band edges, with less attention to other physical parameters such as effective mass. Besides, there is no study to systematically compare the strain effects on bulk and nanostructures.

In this paper, using wurtzite CdX (X = S, Se, Te) as model systems, we perform first-principles calculations to study the influence of uniaxial [0001] strain on the properties of semiconductor bulk and nanowires (NWs), and compare the strain effects on these two phases. The strain induced changes in the atomic structure, band gap, band edge state, and effective mass have been studied. We find that the variations of band gaps for both bulk and NWs under uniaxial strain exhibit similar nonlinear behavior, with a band gap maximum at a critical strain corresponding to band crossing of heavy hole (HH) and crystal hole (CH) bands. However, the critical strain of NWs highly depends on the character of the valence band maximum (VBM) state of the unstrained NWs, which is related to the structural deformation induced by surface contraction. For large $\{10\bar{1}0\}$-faceted NWs with HH-like VBM, the critical strain appears at compressive strain, and the VBM state is mainly localized near the surface. For NWs with $\{11\bar{2}0\}$ facets or small diameters which have CH-like VBM, the critical strain appears at tensile strain, and the VBM state is localized in the core region. The external uniaxial strain can further modify the character of the VBM state, and thus can tune the hole effective mass and its charge distribution. On the other hand, the conduction band minimum (CBM) state of NWs is always localized in the core region, and the electron effective mass exhibits a linear relation with the CBM–HH energy difference, similar to bulk material. Our study can help to understand the structural and electronic properties of NWs under strain, and would provide a guide to synthesize strained nanostructures with desirable physical properties.

The paper is organized as follows. After an introduction in Section 1, the computational method is given in Section 2. In Section 3, we present the details of strain effects on bulk and NWs. The conclusion is given in Section 4.

2. Computational method and models

Our first-principles calculations based on density functional theory (DFT) are performed using the Vienna *ab initio* simulation package (VASP)[25] with generalized gradient approximation of Perdew–Burke–Ernzerhof (PBE)[26] for the exchange–correlation functional. We adopt the projector augmented wave pseudopotential[27] and set the energy cutoff for the plane-wave basis as 320 eV. The Monkhorst–Pack k-points meshes[28] of $8\times8\times8$ and $1\times1\times8$ are used for structural relaxation for bulk and NWs, respectively. All atomic coordinates are fully relaxed until Hellman–Feymann forces on each atom are less than 0.01 eV/Å. Since PBE is well known to underestimate the band gap and effective mass of semiconductors, we employ the modified Becke–Johnson (MBJ) method[29] with split–orbit coupling to obtain a more reliable band gap and effective mass for bulk materials.

In this work, wurtzite CdX bulk (the inset in Fig. 1(a)) and NWs along the [0001] direction with different facets are considered. The vacuum space between NWs is about 15 Å in order to avoid interactions between adjacent images. The NWs with $\{10\bar{1}0\}$ and $\{11\bar{2}0\}$ facets are denoted as (CdX)-n $\{10\bar{1}0\}$ and (CdX)-n $\{11\bar{2}0\}$, respectively, where n is the number of atomic layers in the cross section of the NW. For the two smallest NWs (n = 1 and 2), only the $\{10\bar{1}0\}$ facet is available.

3. Results and discussion

3.1. Bulk materials under uniaxial strain

The lattice parameters, energy band gaps, and effective masses of unstrained CdX bulk are listed in Table 1. The optimized lattice parameters a, c, and u from our calculations are in good agreement with experimental values[6] and previous calculations.[8,30] As is expected, PBE underestimates both the band gap and the effective mass, while MBJ yields an excellent description for the band gap and overestimates the effective mass by about 10%–30%.[29]

Table 1. Structural parameters (a, c, u), band gaps $E_{g,bulk}$, and effective masses m_e^* and m_h^* at the Γ point along the [0001] direction for bulk CdX using PBE and MBJ. Experimental and other calculation results are also listed for comparison.

	Method	a/Å	c/Å	u	$E_{g,bulk}$/eV	m_e^*/m_0	m_{HH}^*/m_0	m_{CH}^*/m_0
CdS	PBE	4.212	6.866	0.376	1.072	0.116	1.783	0.116
	MBJ				2.593	0.234	2.106	0.286
	Expt.[6]	4.136	6.714	0.378	2.582	0.188		
	Other cal.[30]	4.137	6.714	0.375	2.02	0.210	1.53	
CdSe	PBE	4.390	7.175	0.375	0.518	0.054	1.593	0.055
	MBJ				1.780	0.159	1.839	0.222
	Expt.[6]	4.300	7.011	0.376	1.732	0.130		
	Other cal.[30]	4.299	7.015	0.375	1.790	0.18	1.600	
CdTe	PBE	4.681	7.677	0.375	0.599	0.054	1.272	0.054
	MBJ				1.409	0.122	1.297	0.143
	Expt.[6]	4.57	7.470		1.600			
	Other cal.[8]	4.550	7.451	0.375				

To study the strain effects on bulk materials, we consider a wide range of uniaxial strain ε (from -18% compressive to $+6\%$ tensile) along the [0001] direction. Under the anisotropic strain, the atomic structure deviates from the ideal tetrahedral coordinates. With the increase of the c parameter along the [0001] direction, both a and u decrease monotonically, and the volume of the unit cell is gradually expanded. Meanwhile the bond angle α increases and β decreases. With extremely large compression ($\varepsilon = -18\%$), CdSe transforms from the wurtzite phase to a planar graphitelike phase,[31] with α, β, and u close to 90°, 120°, and 0.5, respectively. The bond lengths show more complicated variations under uniaxial strain, as shown in Fig. 1(a). At equilibrium, the axial bond d_1 is slightly longer than the nonaxial bond d_2 for CdSe. From -8% to $+6\%$ uniaxial strain, both d_1 and d_2 increase with parameter c, but at different rates. As seen from Fig. 1(a), d_1 becomes smaller than d_2 at compressive strain $\varepsilon < -1\%$, and both bond lengths reach their minimum values at $\varepsilon = -8\%$. At larger compressive strain ($\varepsilon < -8\%$), both d_1 and d_2 increase with the decrease of the c parameter. Close to the phase transformation point, d_1 even exceeds d_2 at $\varepsilon = -14\%$. Similar structural changes have also been observed for bulk CdS and CdTe.

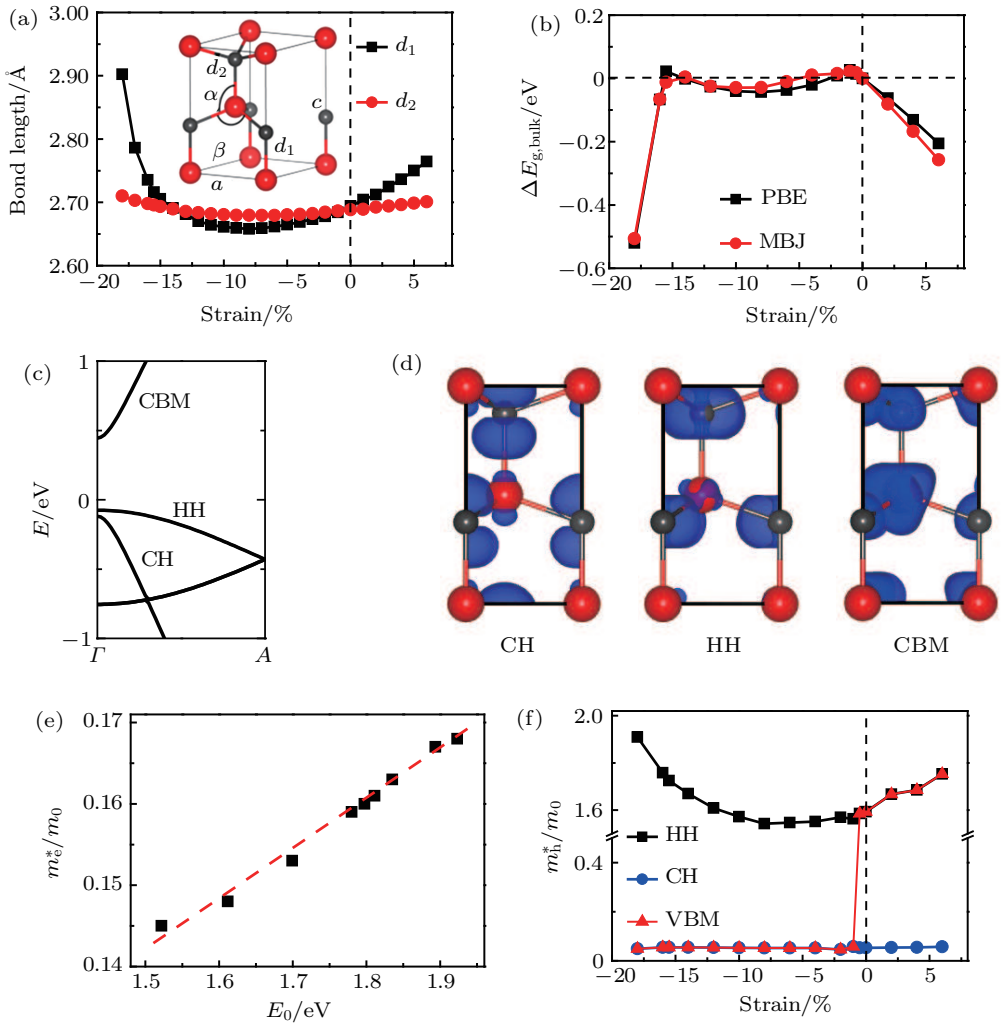


Fig. 1. (color online) The variations of (a) bond lengths d_1 and d_2, and (b) band gap $E_{g,bulk}$ for CdSe bulk as a function of uniaxial [0001] strain. (c) The band structure of unstrained CdSe bulk along the [0001] direction. (d) The isosurfaces of charge density of the CH, HH, and CBM states of unstrained CdSe bulk. The isosurface value is 0.005 e/Å^3. (e) The variation of electron effective mass m_e^* for CdSe bulk as a function of CBM–HH energy difference E_0. (f) The variation of hole effective mass m_h^* for CdSe bulk as a function of uniaxial [0001] strain. The inset in panel (a) shows the atomic structure of the unit cell of wurtzite CdSe bulk. The parameters d_1 and d_2 are the axial and nonaxial bonds, respectively, while α and β denote the bond angles. Red and gray spheres represent Cd and Se atoms, respectively.

Figure 1(b) shows the dependence of the band gap $E_{g,bulk}$ on the uniaxial strain for bulk CdSe calculated with PBE and MBJ. Although PBE underestimates the band gap, it predicts very similar nonlinear variations of the band gap under strain to MBJ. Peng X *et al.* also validated that PBE can correctly predict the band gap variation and the direct-indirect-direct transition under uniaxial strain by comparing to more reliable hybrid functional calculations.[32] As shown in Fig. 1(b), the band gap reduces rapidly with the increase of tensile strain. At compressive strain, the band gap initially increases slightly, reaching a maximum at a critical strain $\varepsilon_C = -1\%$, and then drops with further compression. At $\varepsilon = -8\%$, the band gap is reduced to a local minimum. At large compressive strain (-14% and -15.5% for MBJ and PBE, respectively), VBM is

shifted from Γ to H point. Such direct–indirect band gap transition results in an abrupt decrease of the band gap as shown in Fig. 1(b).

The variation of the band gap is determined by the changes of the band edges under uniaxial strain. The band structure of the unstrained CdSe bulk along [0001] direction is shown in Fig. 1(c). The CBM state is mainly composed of Cd s orbitals and mainly depends on the volume change (see Fig. 1(d)).[33,34] Whereas the HH and CH states at the valence band top highly depend on the crystal field splitting. The HH state is mainly composed of Se p_x and p_y orbitals and closely related to the nonaxial bond d_2, while the CH band mainly consisting of Se p_z orbitals is closely related to the axial bond d_1 (see Fig. 1(d)). At equilibrium with $d_2 < d_1$, the in-plane coupling is stronger than the out-of-plane coupling, and would result in a larger band width for the HH band. Therefore, the HH band (in-plane coupling) is higher than the CH band (out-of-plane coupling) at the Γ point and acts as the VBM.[34]

At compressive strain, CBM goes up due to the decrease of volume, resulting in an increase of the band gap at small compressive strain. However, the decrease of d_1 leads to a stronger out-of-plane coupling and an up-shift of the CH state. At compressive strain $\varepsilon < -1\%$ where $d_1 < d_2$, the CH state exceeds the HH state and becomes the VBM. Because the volume deformation potential is relatively smaller for more ionic CdX,[33] the increase of CH band energy overcomes the increase of CBM, leading to a decrease of band gap when $\varepsilon < -1\%$. We can see that the critical strain $\varepsilon_C = -1\%$ essentially corresponds to the HH–CH band crossing point. At $\varepsilon = -8\%$ where d_1 and d_2 have a maximum difference, the maximum crystal field splitting leads to a local minimum of the band gap. Under tensile strain, the HH band is always the VBM state since $d_2 < d_1$ (Fig. 1(a)). As the increase of tensile strain, CBM goes down due to the increase of volume, and the HH band goes up due to the increased crystal field splitting, leading to a rapid decline in the band gap as shown in Fig. 1(b). Biaxial strain can also induce anisotropic structural deformation of wurtzite semiconductors, and similar HH–CH band crossing has been predicted in the biaxially strained CdX and nitrides.[34]

We further calculate the variation of effective masses at the Γ point under uniaxial strain. Figure 1(e) shows the electron effective mass m_e^* of CdSe bulk as a function of the energy difference between the CBM and HH state (denoted as E_0) calculated by MBJ from -8% to $+6\%$ uniaxial strain. We find a linear relation between m_e^* and E_0, in good agreement with previous studies that the electron effective mass of tetrahedral semiconductors and alloys varies linearly with the band gap.[35] It is worth noting that the linear relation of m_e^* is correlated with E_0 but not with the band gap, due to the HH–CH band crossing induced by uniaxial strain. At larger compressive strain ($\varepsilon < -8\%$), the strained wurtzite structure is significantly deviated from the tetrahetral coordinates, and the relation of m_e^*–E_0 becomes nonlinear (not shown). Figure 1(f) shows the hole effective mass under uniaxial strain for CdSe bulk. The CH effective mass remains almost unchanged, while the HH effective mass shows a nonlinear variation with a minimum at -8% where the largest crystal field splitting results in a minimum curvature of the HH band. Since HH and CH bands cross at the critical strain $\varepsilon_C = -1\%$, we would expect a jump of the VBM effective mass from m_{CH}^* to m_{HH}^* at ε_C. Similar variations of effective masses are also observed for bulk CdS and CdTe. We also notice that the effective mass calculated by PBE is underestimated, but the variation under strain is similar to the MBJ result (not shown). Therefore, we would rely on the PBE method to study the variation of effective masses of NWs in the following.

3.2. Electronic properties of pristine NWs

The lattice parameter c and the band gap E_g as a function of diameter d for CdSe NWs are presented in Fig. 2(a). Due to the surface contraction, the lattice parameter c of NWs is smaller than the bulk value. Among them, the CdX-1 $\{10\bar{1}0\}$ NW has the smallest c parameter because of its largest surface-to-volume ratio. For the same n, the $\{11\bar{2}0\}$-faceted NWs have smaller c parameter than the $\{10\bar{1}0\}$-faceted NWs, indicating stronger contraction imposed by the $\{11\bar{2}0\}$ facets than the $\{10\bar{1}0\}$ facets. Due to quantum confinement, the band gap E_g of NWs reduces monotonically and converges to the value of bulk with the increase of diameter (Fig. 2(a)).[36] Figure 2(b) shows the absolute energies of the band edges for different CdSe NWs using the vacuum level as energy zero. As we can see, the VBM just slightly shifts upwards with increasing diameter, and the decrease of E_g is mainly due to the decline of the CBM energy. Besides, we fit the E_g with a function of $E_{g,bulk} + \text{const} \times (1/d)^\gamma$ for large NWs with $n > 1$.[37] The fitted parameter γ is 0.935, 0.791, and 0.793 for CdS, CdSe, and CdTe NWs, respectively, smaller than the expected value 2 using an effective-mass particle-in-a-box approach.[37] This is because the effective mass is also size dependent as will be discussed later.

The effective masses along the [0001] direction at the band edges for CdSe NWs are shown in Figs. 2(c) and 2(d). Interestingly, m_e^* is in inverse proportion to the diameter except for (CdSe)-1 $\{10\bar{1}0\}$.[38] However, the hole effective mass m_h^* at VBM varies between 0.2 m_0 and 1.5 m_0. For large NWs with $\{10\bar{1}0\}$ facets, m_h^* increases with diameter, converging to the HH effective mass m_{HH}^* of bulk. The VBM state of these NWs is indeed composed of p_x and p_y orbitals and is HH-like. On the other hand, for $\{11\bar{2}0\}$-faceted NWs and the two smallest NWs, m_h^* decreases with increasing diameter, and converges to the CH effective mass m_{CH}^* of bulk. Accordingly, the VBM state of these NWs is found to be CH-like, mainly composed of p_z orbitals.

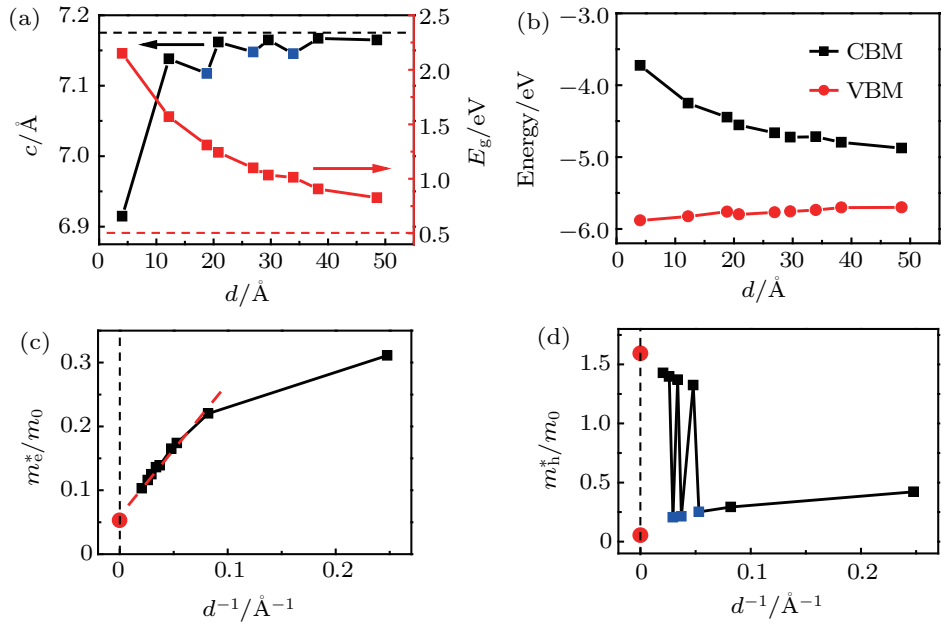


Fig. 2. (color online) The variations of (a) lattice parameter c and band gap E_g, (b) band edge energies, (c) electron effective mass m_e^*, and (d) hole effective mass m_h^* as a function of diameter d for CdSe NWs. The bulk values of c (black) and $E_{g,bulk}$ (red) are also shown as horizontal dashed lines for comparison in panel (a). The bulk effective masses are presented as spheres at $d^{-1} = 0$ in panels (c) and (d). The blue squares denote the NWs with $\{11\bar{2}0\}$ facets in panels (a) and (d). The lines are a guide.

We find that the VBM character is closely related to the average bond lengths. For large $\{10\bar{1}0\}$-faceted NWs with HH-like VBM, the averaged d_1 is larger than the averaged d_2. However, for small NWs or the $\{11\bar{2}0\}$-faceted NWs with CH-like VBM, the averaged d_1 is shorter than the averaged d_2. As seen from Fig. 2(a), these NWs with shorter averaged d_1 also have a smaller c parameter, as a result of stronger surface contraction. We can conclude that the sequence of averaged d_1 and d_2 determines the sequence of HH and CH states for pristine NWs, similar to the strained bulk. In other words, the character of the VBM state highly depends on the size and facets of the pristine NWs due to the different atomic relaxation induced by surface contraction.

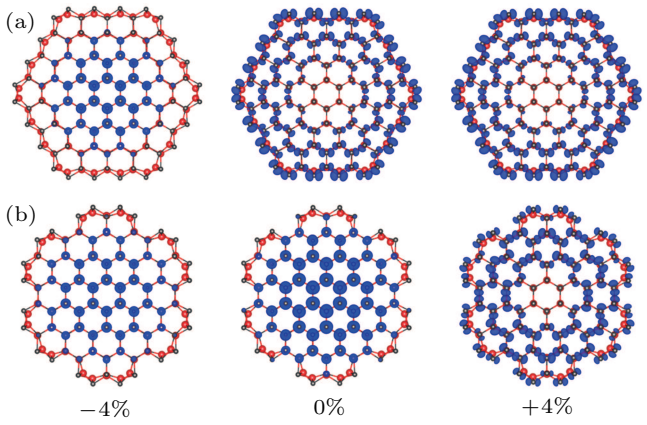


Fig. 3. (color online) Isosurfaces of charge density of the VBM state of (a) (CdSe)-4 $\{10\bar{1}0\}$, and (b) (CdSe)-4 $\{11\bar{2}0\}$ NWs under different uniaxial strains. The isosurface value is 0.0004 e/Å^3.

Moreover, we observed that the CBM state of all CdSe NWs is mainly localized in the core region,[39] while the charge distribution of the VBM state highly depends on its character. The HH-like VBM state is mainly localized near the surface (Fig. 3(a)). Consequently the electron and hole states in these NWs are spatially separated, resembling a type-II band offset in the heterojunctions. However, the CH-like VBM state is mainly localized in the core region and has a large overlap with the CBM state (Fig. 3(b)), similar to a type-I band offset. Similar charge separation or overlap for electron and hole states has been predicted in other NWs.[33,39]

The charge distribution of the band edge states for NWs can be understood by the spatial variation of the bond lengths due to the surface contraction. Since the surface imposes an in-plane contraction to the NW, the nonaxial bond length d_2 near the surface is shorter than that in the core. For instance, for (CdSe)-4 $\{10\bar{1}0\}$ NW, the surface d_2 is 2.679 Å, shorter than d_2 in the core (2.685 Å),[39] resulting in a stronger in-plane coupling and an up-shift of the HH state near the surface. Therefore, the HH state is supposed to be localized near the surface,[33] as shown in Fig. 3(a). On the other hand, the axial bond length d_1 in the subsurface layer is elongated due to surface buckling. For (CdSe)-4 $\{11\bar{2}0\}$ NW, the subsurface d_1 (2.701 Å) is longer than that in the core region (2.688 Å). Correspondingly, the weaker out-of-plane coupling results in a down-shift of the CH state near the surface. Therefore, the CH state is mainly localized at the core region, as shown in Fig. 3(b). Besides, the CBM state tends to bend upwards near the surface due to the surface contraction and thus is mainly localized in the core region.[39]

For CdTe and most of CdS NWs, similar relations have

been observed, i.e., the bond lengths determine the VBM character, the charge distribution of the band edge states and the effective mass. However, we observe strong HH–CH mixing of the VBM states for (CdS)-n $\{11\bar{2}0\}$ NWs with $n > 3$. Their VBM states are composed of p_x and p_z orbitals, and the VBM effective masses are about 1.1 m_0–1.2 m_0, between the bulk values of $m^*_{\mathrm{CH}} = 0.116\, m_0$ and $m^*_{\mathrm{HH}} = 1.783\, m_0$. For these CdS NWs, the energies of the HH and CH states at the Γ point are quite similar, with a difference less than 0.01 eV. This could be the reason for the significant HH–CH mixing. For other NWs, the HH–CH energy difference at the Γ point is much larger, and no noticeable HH–CH mixing is observed.

3.3. Strain effects on NWs

Next we discuss the effects of uniaxial strain ε on the electronic properties of NWs. Similar to bulk, the band gap of CdSe NW exhibits a nonlinear variation under uniaxial strain,[33,40] with a maximum at the critical strain ε_{C} as shown in Fig. 4(a). Interestingly, the critical strain ε_{C} highly depends on the character of the VBM state. For NWs with an HH-like VBM state, the critical strain ε_{C} appears at the compressive strain, between -1% and 0%. For NWs with a CH-like VBM state, the critical strain appears at tensile range and approaches to 0% with the increase of diameter.

In order to understand the band gap variations, figure 4(b) shows the band edge energies under uniaxial strain for (CdSe)-4 $\{10\bar{1}0\}$ and (CdSe)-4 $\{11\bar{2}0\}$ NWs, setting the vacuum level as energy zero. As the increase of the parameter c, the CBM state is expected to shift downwards due to the increase of volume. Meanwhile, the HH band shifts upwards and the CH band shifts downwards.[33] For both NWs, there is a crossing between HH and CH bands at the critical strain ε_{C}, corresponding to the maximum of the band gap, similar to the bulk case. For (CdSe)-4 $\{10\bar{1}0\}$ and other NWs with an HH-like VBM, the HH state is higher than the CH state for unstrained NWs, and the HH–CH band crossing point appears at compressive strain near -1%, as shown in Fig. 4(b). On the other hand, for (CdSe)-4 $\{11\bar{2}0\}$ and other NWs with a CH-like VBM, the CH state is higher than the HH state for unstrained NWs, and the HH–CH band crossing point appears at tensile strain (Fig. 4(b)). Similar to the bulk, the character of the VBM state of strained NWs is related to the difference between the averaged d_1 and d_2. At $\varepsilon < \varepsilon_{\mathrm{C}}$ when the CH state is the VBM, the averaged d_1 is shorter than the averaged d_2. However, at $\varepsilon > \varepsilon_{\mathrm{C}}$ when the HH state acts as the VBM, the averaged d_1 becomes larger than the averaged d_2.

The uniaxial strain can also modulate the charge distributions of electron and hole states. The CBM state is localized in the core region under both compressive and tensile strain, and tends to be more delocalized as the lattice parameter c increases.[39] However, the charge distribution of the VBM state is strain dependent, due to the HH–CH band crossing. Under compressive strain $\varepsilon < \varepsilon_{\mathrm{C}}$ when CH acts as the VBM, the VBM state is localized at the core region,[33] exhibiting a type-I level alignment (Figs. 3(a) and 3(b)). Under tensile strain $\varepsilon > \varepsilon_{\mathrm{C}}$ when HH acts as the VBM, the VBM state is localized near the surface,[33] exhibiting a type-II level alignment (Figs. 3(a) and 3(b)). In other words, we can tune the level alignment of the NWs by applying uniaxial strain, regardless of the original level alignment type of the unstrained NWs.

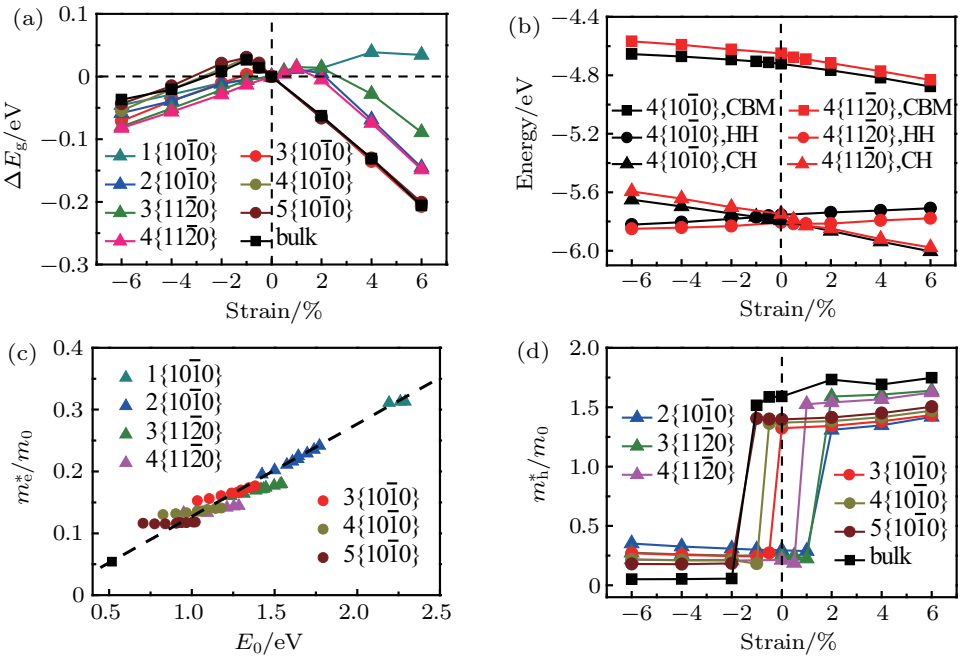


Fig. 4. (color online) The strain-induced changes in (a) band gap E_{g}, (b) band edge energies, and (d) hole effective mass m_{h}^* for CdSe NWs. (c) The electron effective mass m_{e}^* at CBM as a function of CBM–HH band energy difference E_0 for CdSe NWs. The band gaps and effective masses for bulk CdSe are presented by black squares for comparison in panels (a), (c), and (d).

Figures 4(c) and 4(d) show the electron and hole effective masses under uniaxial strain for CdSe NWs. The electron effective mass at CBM is almost linear to E_0 (the CBM–HH energy difference) for all the considered NWs,[38] the same as bulk. Therefore the electron effective mass of NWs can be estimated from the linear m_e^*–E_0 relation of bulk. However, the hole effective mass m_h^* at VBM has an abrupt change from m_{CH}^* to m_{HH}^* at the critical strain ε_C, due to the HH–CH band crossing (Fig. 4(d)).[40] As parameter c increases, the CH effective mass slightly decreases while the HH effective mass gradually increases.

For CdTe and most CdS NWs, we find similar variations of the band gaps, effective masses, and charge distributions of electron and hole states under uniaxial strain. However, for (CdS)-n $\{11\bar{2}0\}$ NWs with $n > 3$, the variation of the VBM state is more complicated. As discussed above, the VBM state of these unstrained CdS NWs is an HH–CH mixed state, and the hole effective mass is between m_{HH}^* and m_{CH}^* of bulk. At small uniaxial strain ($0 < \varepsilon < \varepsilon_C$), the VBM state remains similar to the unstrained case. However, larger uniaxial strain removes the hybridization between the HH and CH states by increasing the HH–CH energy difference at the Γ point. As a result, at compressive strain $\varepsilon < 0$, the VBM is mainly composed of p_z orbitals and is CH-like. Correspondingly, the hole effective mass drops down to about 0.3 m_0. At tensile strain $\varepsilon > \varepsilon_C$, the VBM is mainly composed of p_x and p_y orbitals, and becomes HH-like. The hole effective mass shifts up to about 1.7 m_0.

4. Conclusion

The structural deformation and electronic properties of wurtzite CdX (X = S, Se, Te) bulk materials and NWs along the [0001] direction under [0001] uniaxial strain are systematically investigated using first-principles calculations. Under uniaxial strain, the electron effective mass of the NWs shows the same linear relation with E_0 (CBM–HH energy difference) as the bulk material, and the CBM state is always localized in the core region. On the other hand, the VBM state of NWs exhibits more complicated behavior due to the HH–CH band crossing. The strain-induced changes in band gap and hole effective mass at the VBM for both bulk and NWs are highly nonlinear, with a turning point at the critical strain. However, unlike the bulk phase, the critical strain of NWs is determined by the character of the VBM state of the unstrained NWs. Due to the surface contraction, large NWs with $\{10\bar{1}0\}$ facets have an HH-like VBM state that is localized near the surface, and have a compressive critical strain. Whereas the NWs with $\{11\bar{2}0\}$ facets or small diameters have a CH-like VBM state that is localized in the core, and the critical strain appears at tensile range. Due to the strain induced HH–CH band crossing, the charge distribution of the VBM state can be modified by uniaxial strain, and thus electron–hole separation or overlap can be realized by applying external strain. Our calculations show that the VBM-related properties of NWs depend on its size, facet, and material, which could not be directly derived from the properties of the bulk phase. This study would help to understand the strain effects on the electronic properties of nanostructures, and would provide a theoretical guide to modify the properties of nanostructures by external uniaxial strain.

Acknowledgment

The authors thank Prof. Junwei Luo for our useful discussion and suggestions. All calculations were performed on the TH-1A supercomputer at the National Supercomputing Center in Tianjin, China.

References

[1] Murray C B, Norris D J and Bawendi M G 1993 *J. Am. Chem. Soc.* **115** 8706
[2] Peng X, Schlamp M C, Kadavanich A V and Alivisatos A P 1997 *J. Am. Chem. Soc.* **119** 7019
[3] Huynh W U, Dittmer J J and Alivisatos A P 2002 *Science* **295** 2425
[4] Wang G, Yang X, Qian F, Zhang J Z and Li Y 2010 *Nano Lett.* **10** 1088
[5] Poplawsky J D, Guo W, Paudel N, Ng A, More K, Leonard D and Yan Y 2016 *Nat. Commun.* **7** 12537
[6] Landolt-Boörnstein 1982 *Numerical Data and Functional Relationships in Science and Technology*, New Series (New York: Springer) Group III, Vols. 17a and 22a
[7] Wei S H, Zhang S B and Zunger A 2000 *J. Appl. Phys.* **87** 1304
[8] Wei S H and Zhang S B 2000 *Phys. Rev. B* **62** 6944
[9] Kim S, Fisher B, Eisler H J and Bawendi M 2003 *J. Am. Chem. Soc.* **125** 11466
[10] Zeng Q, Kong X, Sun Y, Zhang Y, Tu L, Zhao J and Zhang H 2008 *J. Phys. Chem. C* **112** 8587
[11] Schäffler F 1997 *Semicond. Sci. Technol.* **12** 1515
[12] Ng W L, Lourenço M A, Gwilliam R M, Ledain S, Shao G and Homewood K P 2001 *Nature* **410** 192
[13] Fischetti M V and Laux S E 1996 *J. Appl. Phys.* **80** 2234
[14] Chuang S L and Chang C S 1996 *Phys. Rev. B* **54** 2491
[15] Grundmann M, Stier O and Bimberg D 1995 *Phys. Rev. B* **52** 11969
[16] Smith A M, Mohs A M and Nie S 2009 *Nat. Nanotechnol.* **4** 56
[17] Ertekin E, Greaney P A, Chrzan D C and Sands T D 2005 *J. Appl. Phys.* **97** 114325
[18] Raychaudhuri S and Yu E T 2006 *J. Vac. Sci. Technol. B* **24** 2053
[19] Yang S, Prendergast D and Neaton J B 2010 *Nano Lett.* **10** 3156
[20] Balet L P, Ivanov S A, Piryatinski A, Achermann M and Klimov V I 2004 *Nano Lett.* **4** 1485
[21] Fu H, Wang L W and Zunger A 1998 *Phys. Rev. B* **57** 9971
[22] Pokatilov E P, Fonoberov V A, Fomin V M and Devreese J T 2001 *Phys. Rev. B* **64** 245328
[23] Sarkar P, Springborg M and Seifert G 2005 *Chem. Phys. Lett.* **405** 103
[24] Peng X and Logan P 2010 *Appl. Phys. Lett.* **96** 143119
[25] Kresse G and Furthmüller J 1996 *Phys. Rev. B* **54** 11169
[26] Perdew J P, Burke K and Ernzerhof M 1996 *Phys. Rev. Lett.* **77** 3865
[27] Blöchl P E 1994 *Phys. Rev. B* **50** 17953
[28] Monkhorst H J and Pack J D 1976 *Phys. Rev. B* **13** 5188
[29] Kim Y S, Marsman M, Kresse G, Tran F and Blaha P 2010 *Phys. Rev. B* **82** 205212
[30] Xu Y N and Ching W Y 1993 *Phys. Rev. B* **48** 4335
[31] Yadav S K, Sadowski T and Ramprasad R 2010 *Phys. Rev. B* **81** 144120
[32] Peng X, Wei Q and Copple A 2014 *Phys. Rev. B* **90** 085402
[33] Wu Y, Chen G, Wei S H, Al-Jassim M M and Yan Y 2011 *Appl. Phys. Lett.* **99** 262103
[34] Yang S, Prendergast D and Neaton J B 2011 *Appl. Phys. Lett.* **98** 152108
[35] Shantharama L G, Adams A R, Ahmad C N and Nicholas R J 1984 *J. Phys. C: Solid State Phys.* **17** 4429
[36] Li J and Wang L W 2005 *Phys. Rev. B* **72** 125325
[37] Zhao X, Wei C M, Yang L and Chou M Y 2004 *Phys. Rev. Lett.* **92** 236805
[38] Persson M P and Xu H Q 2004 *Nano Lett.* **4** 2409
[39] Kou L, Li C, Zhang Z Y, Chen C and Guo W 2010 *Appl. Phys. Lett.* **97** 053104
[40] Huan H, Chen L and Ye X 2017 *Nanoscale Res. Lett.* **12** 178